

Durham Research Online

Deposited in DRO:

01 November 2018

Version of attached file:

Accepted Version

Peer-review status of attached file:

Peer-reviewed

Citation for published item:

Eaves, Shaun R. and Collins, Julia A. and Jones, R. Selwyn and Norton, Kevin P. and Tims, Stephen G. and Mackintosh, Andrew N. (2018) 'Further constraint of the in situ cosmogenic ^{10}Be production rate in pyroxene and a viability test for late Quaternary exposure dating.', *Quaternary geochronology.*, 48 . pp. 121-132.

Further information on publisher's website:

<https://doi.org/10.1016/j.quageo.2018.09.006>

Publisher's copyright statement:

© 2018 This manuscript version is made available under the CC-BY-NC-ND 4.0 license
<http://creativecommons.org/licenses/by-nc-nd/4.0/>

Additional information:

Use policy

The full-text may be used and/or reproduced, and given to third parties in any format or medium, without prior permission or charge, for personal research or study, educational, or not-for-profit purposes provided that:

- a full bibliographic reference is made to the original source
- a [link](#) is made to the metadata record in DRO
- the full-text is not changed in any way

The full-text must not be sold in any format or medium without the formal permission of the copyright holders.

Please consult the [full DRO policy](#) for further details.

Further constraint of the *in situ* cosmogenic ^{10}Be production rate in pyroxene and a viability test for late Quaternary exposure dating

Shaun R. Eaves^{a*}, Julia A. Collins^b, R. Selwyn Jones^c, Kevin P. Norton^d, Stephen G. Tims^e, Andrew N. Mackintosh^{a,d}

^a*Antarctic Research Centre, Victoria University of Wellington, PO Box 600, 6140 Wellington, New Zealand*

^b*GNS Science, Gracefield, Lower Hutt, Wellington, New Zealand*

^c*Department of Geography, Durham University, Solsmes Road, Durham, DH1 3LE, UK*

^d*School of Geography Environment and Earth Science, Victoria University of Wellington, PO Box 600, 6140 Wellington, New Zealand*

^e*Department of Nuclear Physics, Research School of Physics and Engineering, The Australian National University, Canberra, ACT 2601, Australia*

*Corresponding author: shaun.eaves@vuw.ac.nz

Abstract

Beryllium-10 (^{10}Be) in quartz represents the most common *in situ* cosmogenic nuclide used for quantifying Earth-surface processes, primarily due to the prevalence of quartz in the Earth's crust. However many landscapes lack quartz-bearing rocks, thus other nuclide-mineral pairs are required for geochronometric and geomorphic applications. Here we describe the successful isolation and measurement of *in situ* ^{10}Be concentrations in pyroxene from two mafic sample sets: (i) andesite boulders of the Murimotu Formation debris avalanche on Mt. Ruapehu, New Zealand, and (ii) dolerite cobbles deposited in a ~100 m vertical transect at Mt. Gran by Mackay Glacier, Antarctica. Precise radiocarbon age constraint of the New Zealand site provides further geological constraint of the reference (at sea level and high latitude) ^{10}Be production rate in pyroxene, which we find to be indistinguishable from a previous estimate. Combining our results with previous data yields a reference production rate of $3.2 \pm 0.8 \text{ at. g}^{-1} \text{ yr}^{-1}$ ($n=5$; 'Lm' scaling). Application of this rate to the glacial cobbles at Mackay Glacier yields a relatively coherent chronology of ice surface lowering between ~14 and 6 ka, which is broadly consistent with a well-constrained quartz-based ^{10}Be chronology from nearby

nunataks. Improving the viability of *in situ* ^{10}Be for geological applications in mafic domains requires increased analytical precision beyond current levels. This improvement may be best achieved by further modification of the quartz-based methodologies for ^{10}Be purification, in order to better handle the high cationic contaminant loads of ferromagnesian minerals. In addition, further ^{10}Be measurements from suitable mafic sedimentary deposits with independent age control (e.g. existing cosmogenic ^3He calibration sites) will help to refine estimates of the reference production rate.

Keywords: ^{10}Be ; pyroxene; sequential leaching; cosmogenic nuclides; production rate calibration.

1. Introduction

Accumulation of cosmogenic nuclides in minerals at Earth's surface, via interaction with galactic radiation, provides an important tool for constraining the timing and rates of surficial processes over geologic timescales (Gosse and Phillips, 2001). Advances in chemical extraction procedures, mass spectrometry and understanding of cosmogenic nuclide production rates have resulted in this technique becoming the premier method for a host of geochronometric applications (see von Blanckenburg and Willenbring, 2014 for a recent overview). Beryllium-10 (^{10}Be) in quartz represents the most commonly-used *in situ* nuclide-mineral pair for several reasons. The chemical structure of quartz (SiO_2) means that production of *in situ* ^{10}Be is relatively simple, with little scope for compositional variability. Quartz also lacks cleavage, which reduces the surface available for meteoric ^{10}Be adsorption and means that this potential contaminant can be readily removed by simple acid leaching procedures. Furthermore, as the second-most abundant mineral in Earth's crust, quartz is often available in sufficient quantities for surface exposure applications. However there are some geological domains where this latter point is not true (e.g. intermediate-mafic lavas). In these situations other cosmogenic nuclides and/or mineral phases are required for surface exposure dating applications.

Cosmogenic nuclide applications in mafic terrains have thus far largely been limited to cosmogenic helium-3 (^3He) in pyroxene and olivine (Goehring et al., 2010), neon-21 (^{21}Ne) in olivine/pyroxene (Schäfer et al., 1999; Fenton et al., 2009), and chlorine-36 (^{36}Cl) in whole

rock and feldspar (Schimmelpfennig et al., 2011). More recently, Zerathe et al. (2017) demonstrated the suitability of feldspar for *in situ* ^{10}Be applications. While there are numerous examples of the successful application of these nuclides, the production pathways can be complex and, in the case of ^3He and ^{21}Ne , precise determination of cosmogenic concentrations requires deconvolution from non-cosmogenic sources (Niedermann, 2002). Expanding the range of nuclides and target minerals available for cosmogenic applications therefore represents an important objective for geochronological research.

Previous attempts to measure *in situ* ^{10}Be in ferromagnesian phases have had mixed results. Nishiizumi, et al. (1990) obtained comparable exposure ages from a range of nuclides, including *in situ* ^{10}Be , in olivines from Hawaiian lava flows. Meanwhile Seidl et al. (1997) briefly described a successful methodology involving repeated dilute HF-HCl leaching to track meteoric ^{10}Be removal from olivines in a Hawaiian basalt. However, Ivy-Ochs, et al. (1998) concluded that sequential dissolution did not remove meteoric ^{10}Be from pyroxene crystals and suggested that weathering and clay formation may allow meteoric ^{10}Be to penetrate the grain interior of this mineral. Blard et al. (2008) proposed a pre-leaching crushing step designed to increase the surface area of the pyroxene crystals for more effective removal of meteoric ^{10}Be via sequential acid leaches. The successful leaching experiments presented by Blard et al. (2008) demonstrated the potential viability for robust measurements of *in situ* ^{10}Be in pyroxene.

In this study we take advantage of recent field campaigns at mafic domains in both New Zealand (Eaves et al., 2015) and Antarctica (Jones et al., 2015), which have yielded samples with sufficient pyroxene content for evaluating the protocol for chemical isolation of *in situ* ^{10}Be in pyroxene (cf. Blard et al., 2008). An additional benefit of these study sites is the support from independent chronological data concerning exposure duration, derived from radiocarbon (New Zealand) and *in situ* ^{10}Be in quartz (Antarctica) – described more fully in Section 2. These additional data enable further constraint of the reference production rates of *in situ* ^{10}Be in pyroxene, as well as evaluation of the viability of this nuclide-mineral pair for exposure dating applications.

2. Study sites

2.1 Murimotu Formation debris avalanche, Mt Ruapehu, New Zealand

101 Mount Ruapehu (2797 m asl; 39.28°S, 175.56°E) is an andesite-dacite stratovolcano situated
102 in central North Island, New Zealand, at the southern margin of the Taupo Volcanic Zone
103 (Figure 1; Townsend et al., 2017). The present-day relief of the cone and distribution of
104 sediment forming the surrounding ringplain reflects the interplay of volcanism, erosion and
105 deposition by glaciers and rivers, and mass movement events since ~300 ka (Conway et al.,
106 2016; Eaves et al., 2015, 2016a,b, Tost and Cronin, 2016).

107
108 Here we target the Murimotu Formation – a hummocky debris avalanche deposit on the lower
109 NW flank of Mount Ruapehu (Palmer and Neall, 1989), where 8 radiocarbon dates from
110 organic material that was entrained within, or buried beneath, the debris avalanche material
111 constrain the timing of this event to $10,535 \pm 110$ cal. yr BP (Eaves et al., 2015). In the same
112 study, Eaves et al. (2015) combined this precise new age with measurements of cosmogenic
113 ^3He in pyroxenes from large (~1-10 m high) surficial blocks deposited during the debris
114 avalanche event, which verified the globally-derived cosmogenic ^3He production rate (e.g.
115 Goehring et al. 2010) for applications in New Zealand (e.g. Eaves et al. 2016b). We take
116 advantage of the precise independent chronological data and coexisting cosmogenic ^3He
117 concentrations for the Murimotu Formation to calibrate *in situ* cosmogenic ^{10}Be production in
118 pyroxene.

119
120 Sufficient pyroxene separates remained from the ^3He analyses of Eaves et al. (2015) for three
121 samples (MM1201, MM1202, and MM1204). For MM1203 we processed a separate sample
122 taken from the same boulder as in Eaves et al. (2015). This later sample was collected from a
123 position on the boulder surface immediately adjacent to the earlier sample site (Figure 2a).
124 Sample locations and characteristics of all samples used in this study are given in Table 1, with
125 elemental composition of Murimotu samples in the Supplementary Data File.

126
127 Due to short supply of pyroxenes from the Murimotu clasts we sought to test the ^{10}Be isolation
128 procedure of Blard et al. (2008) using a separate sample, of similar lithology, that has been
129 exposed for sufficient time to acquire measurable quantities of *in situ* ^{10}Be . For this purpose
130 we used a moraine boulder – here labelled JC2 - from a glaciated valley situated on the south
131 west flank of Mt Ruapehu (Figure 1, 2b), which, based on glacier modelling experiments and
132 morphostratigraphic correlation to dated moraine sequences nearby, is thought to have been
133 deposited at or shortly after the Last Glacial Maximum (Eaves et al., 2016c).

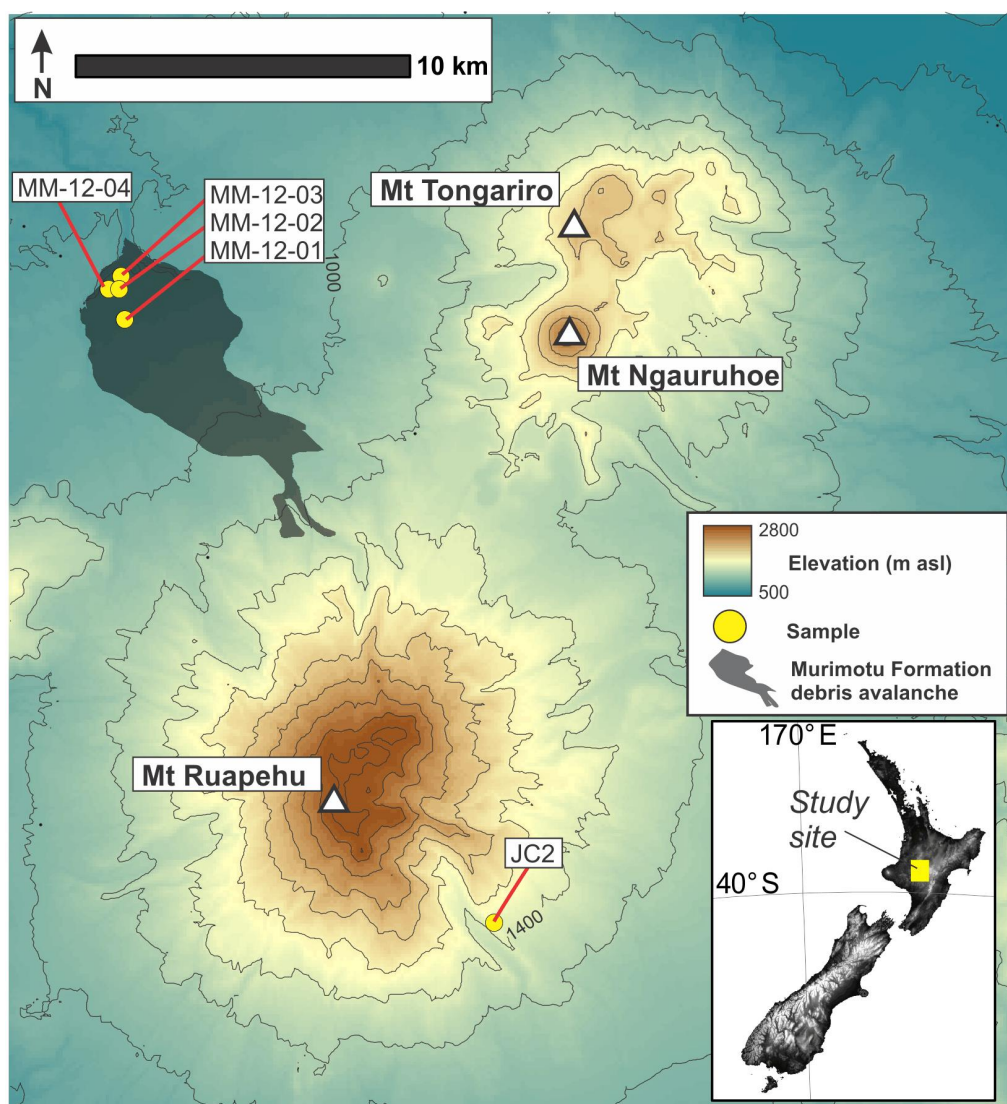


Figure 1: Topographic setting and sample distribution at Mt Ruapehu.

JC2 ¹	-39.318	175.614	1483	1.03E+05 ^a	1.3E+04 ^a	0.999	2.7	2.0	- ^a
<i>Murimotu Formation, Mt Ruapehu</i>									
MM1201 ²	-39.156	175.478	855	5.67E+04	1.2E+04	0.999	2.7	2.5	2.76
MM1202 ²	-39.148	175.475	820	9.12E+04	1.7E+04	0.999	2.7	3.5	2.83
MM1203 ²	-39.144	175.476	809	1.36E+05	1.8E+04	0.999	2.7	2.0 ^b	2.35
MM1204 ²	-39.148	175.473	818	6.88E+04	1.4E+04	0.999	2.7	2.0	2.24
<i>Mt Gran, Mackay Glacier, Antarctica</i>									
MG30 ²	-76.997	161.042	1043	1.83E+05	3.7E+04	0.986	3.0	2.0	1.49
MG32 ³	-76.997	161.041	1043	1.45E+05	5.5E+04	0.986	3.0	3.5	1.66
MG07 ³	-76.998	161.039	1022	3.62E+05	9.3E+04	0.989	3.0	1.8	1.23
MG12 ²	-76.999	161.038	1013	1.32E+05	3.7E+04	0.979	3.0	5.8	1.09
MG15 ³	-76.999	161.040	997	1.95E+05	5.2E+04	0.985	3.0	3.8	1.26
MG19 ³	-76.999	161.041	981	1.05E+05	5.8E+04	0.988	3.0	4.0	1.26
MG22 ³	-76.999	161.043	976	1.00E+05	3.9E+04	0.985	3.0	4.6	1.46
MG01 ³	-76.999	161.042	970	5.95E+04	4.3E+04	0.975	3.0	1.5	1.29

^a Weighted mean of multiple post-HF leaching rounds (see Table 2)

^b Thickness differs from that reported in Eaves et al. (2015) as a different surface sample (from the same parent boulder) was used for this study.

2.2 Mt Gran, Mackay Glacier, Antarctica

Mackay Glacier is an outlet of the East Antarctic Ice Sheet, draining through the Transantarctic Mountains to the Ross Sea (Figure 3). Glaciation in this region since at least ~15 Ma has formed erosional surfaces and deposited thin drapes of diamict near to the modern ice margins (Sugden and Denton, 2004). The recent glacial history of Mackay Glacier was determined using surface exposure dating of glacially-deposited cobbles that were sampled in transects extending above the modern ice surface (Jones et al., 2015). By measuring ¹⁰Be in quartz, Jones et al. (2015) produced a chronology of ice surface lowering from ~22 ka to near-present. The most notable episode of lowering was recorded at Mt Suess, located on the southern side of the glacier (Figure 3b), where >230 m of rapid thinning occurred at ~7 ka BP.

Mt Gran (2233 m asl; 76.98°S 160.98°E) is an ice-free massif situated on the northern side of Mackay Glacier, ~26 km upstream from the present-day grounding line (Figure 3b,d). The local bedrock primarily comprises Ferrar Dolerites of the Beacon Supergroup (Mirsky et al., 1965). Adjacent to the ice margin, dolerite cobbles displaying evidence for glacial transport can be found perched on glacially-rounded and striated bedrock and record past ice surface lowering at this site (Figure 2c-f). Eight sub-rounded to sub-angular dolerite cobbles were collected in January 2013 between 970 and 1043 m asl (Figure 3d). The underlying bedrock surfaces had

168 varying degrees of fragmentation, pitting and oxidisation, with sporadic areas of ~1 mm-deep
169 striae. The cobble surfaces had sub-millimetre scale weathering, with negligible to major
170 oxidisation. Plagioclase is the most abundant mineral (~80%) in these dolerites, pyroxenes
171 make up 10-20%, and the remaining ~10% other accessory minerals. The pyroxenes are
172 primarily clinopyroxene with small amounts of orthopyroxene, are up to 4 mm in length, and
173 contain some signs of alteration that differ between the samples.

174
175 Glacier flowline modelling indicates that ice thickness in the vicinity of Mt Gran has a similar
176 sensitivity to grounding line retreat to the nunataks in the lower Mackay Glacier targeted by
177 Jones et al. (2015) (Figure 3c). This suggests that our sample transect from Mt. Gran should
178 also capture ice surface lowering between the Last Glacial Maximum and present, and thus
179 affords the opportunity to evaluate the viability of this mineral-nuclide pair for late Quaternary
180 exposure dating applications. To reduce the potential for scaling-based biases influencing this
181 test, we use the Jones et al. (2015) chronology calculated using the New Zealand based
182 calibration of ^{10}Be production in quartz (Putnam et al., 2010) – see Supplementary Data File.

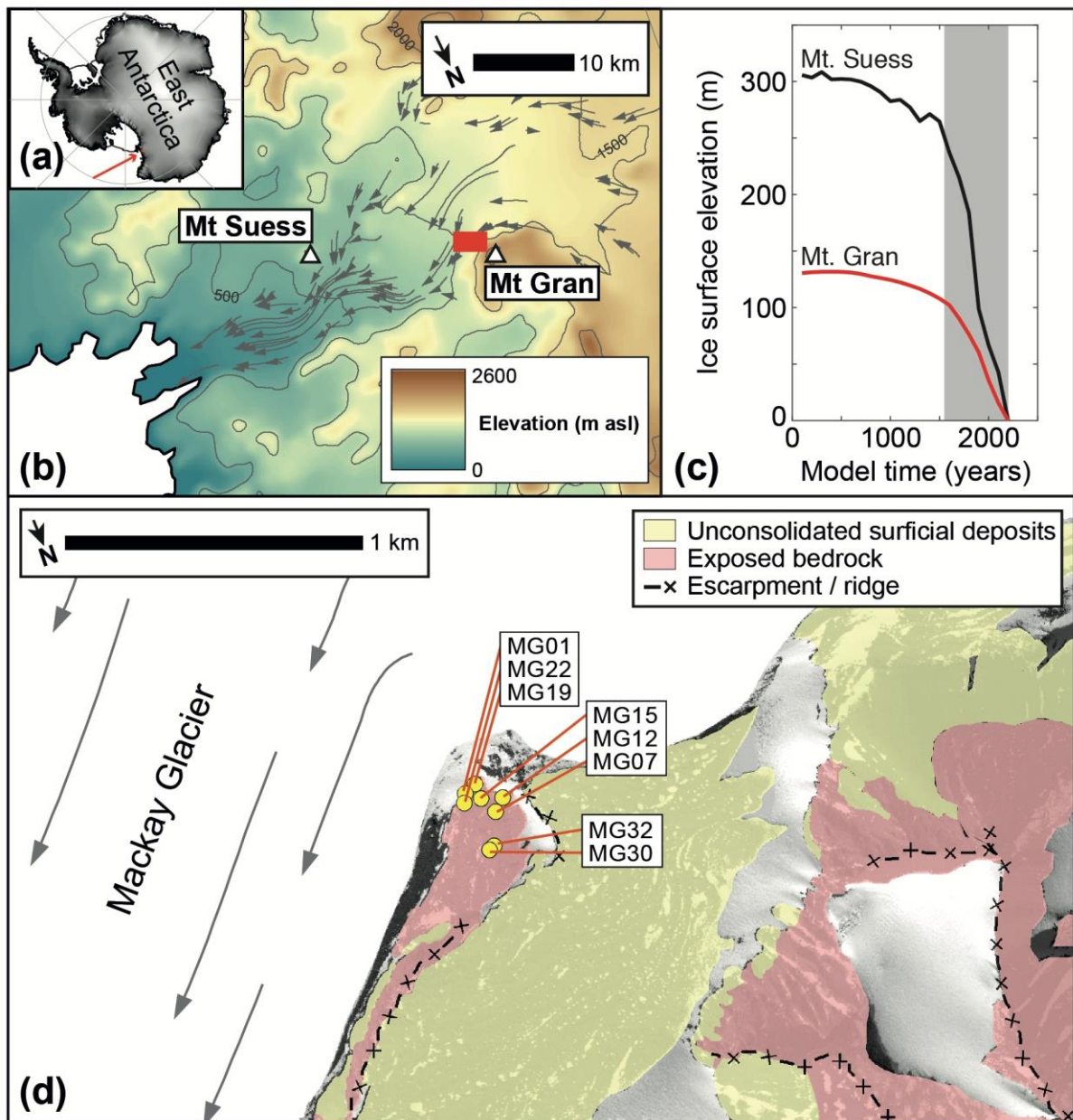


Figure 3: Topographic setting and sample distribution at Mt. Gran. a) Location of Mackay Glacier is shown with a red arrow. b) Mt. Gran and Mt. Suess lie either side of the main Mackay Glacier trunk. Grey arrows denote glacier flowstripes. c) Trends of modelled ice surface lowering is similar at Mt. Gran and Mt. Suess (Jones et al., 2015), with both sites experiencing rapid thinning at the same time (grey area). d) Samples at Mt. Gran were collected from a region of rounded bedrock adjacent to the modern ice.

3 Methods

3.1 Mineral separation and meteoric ^{10}Be removal

194
195 We isolated pyroxene from bulk rock via standard magnetic and density separation procedures.
196 Crushed samples were sieved to 125–250 μm and rinsed in distilled water to remove fine
197 particulate matter. Density separation using methylene iodide yielded a heavy fraction ($> 3.1 \text{ g}$
198 cm^{-3}) of ~95 % pyroxene crystals. We then used a hand magnet to remove magnetite and any
199 other strongly magnetic phases, followed by repeated passes under a Frantz Isodynamic
200 Separator to achieve pure pyroxene splits.

201
202 For removal of meteoric ^{10}Be , we followed the leaching protocol outlined by Blard et al. (2008).
203 Clean pyroxene separates were first crushed to $< 90 \mu\text{m}$ using an agate ring mill and a pestle
204 and mortar. This additional crushing step exposes weathering pits and increases the surface
205 area to allow effective removal of meteoric ^{10}Be via successive leaches in 0.04 M
206 hydroxylammonium chloride ($\text{NH}_2\text{OH}.\text{HCl}$), 1M hydrochloric acid (HCl), and 4M
207 hydrofluoric acid (HF) (Blard et al., 2008).

208
209 We tracked meteoric ^{10}Be removal by measuring ^{10}Be concentrations throughout the leaching
210 process (Figure 4, Table 2). Figure 3a shows that ^{10}Be concentrations were reduced by 3 orders
211 of magnitudes after successive leaches in $\text{NH}_2\text{OH}.\text{HCl}$, HCl , and two rounds of HF . Further
212 HF leaches reduced ^{10}Be concentrations by approximately 3 orders of magnitude from c. 10^8
213 at. g^{-1} to c. 10^5 at. g^{-1} . Measurements of ^{10}Be after 3, 4, and 7 rounds of HF leaches (HF leaches
214 1, 5 and 6 were not measured due to failure of subsequent chemical processing) yield
215 concentrations that are indistinguishable from HF_2 ($\chi^2=2.3$, 3d.f. $p>.05$; Figure 4b), which
216 indicates full removal of meteoric ^{10}Be and thus represents the *in situ* ^{10}Be hosted in the
217 pyroxene crystal lattice.

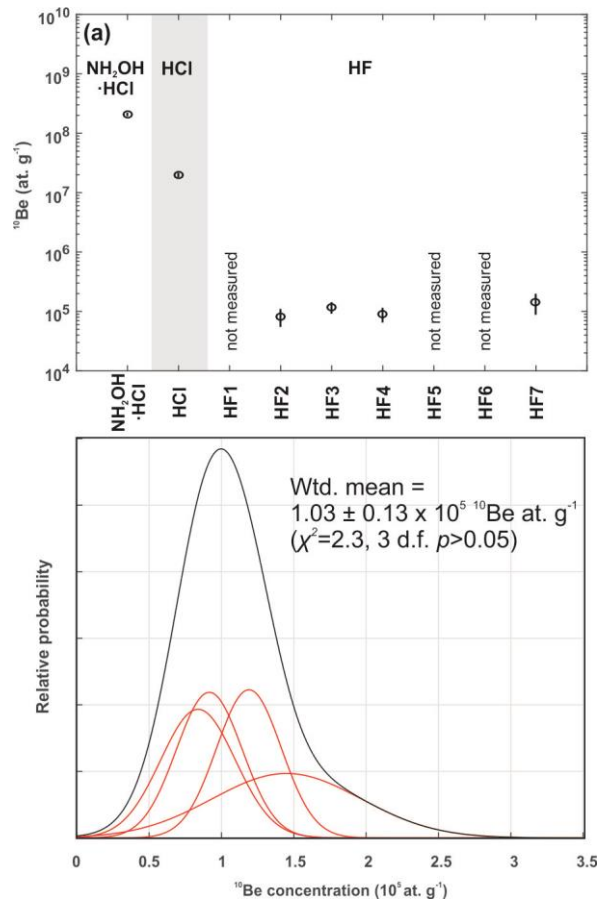


Figure 4: (a) ^{10}Be concentrations after leaching steps; (b) kernel density estimates of ^{10}Be concentrations from leaching steps HF2-4 and HF7 using sample JC2 (red), with the summed estimate of the individual measurements shown in black.

Table 2: Beryllium data for leaching experiments undertaken on sample JC2.

Name	Pyroxene (g)	^9Be (ug)	Measured $^{10}\text{Be}/^9\text{Be}$ (10^{-14} at.at. $^{-1}$)	Blank-corrected $^{10}\text{Be} \pm 1 \sigma$ (10^5 at.)
NOH2HCL	0.0445	413.9	32.73 ± 1.368	2029 ± 87.48
HCl	0.1317	414.4	9.449 ± 0.565	196.8 ± 12.09
HF2	2.1602	413.9	0.746 ± 0.194	0.838 ± 0.258
HF3	2.2591	413.6	1.066 ± 0.176	1.192 ± 0.224
HF4	2.7181	413.4	0.993 ± 0.219	0.916 ± 0.229
HF7	0.8499	413.4	0.538 ± 0.150	1.449 ± 0.515

3.2 Ion exchange chemistry and accelerator mass spectrometry

Following ^9Be carrier addition and dissolution in HF, samples were dried down leaving a fluoride cake where Be was bound to F to form the water soluble compound BeF_2 . This water leach step reduces the concentration of insoluble contaminants (e.g. Na, Al, Mg, Ca) (Stone,

1998). We added 10ml H₂O to fluoride cakes and heated at 60°C for 20 min before cooling and removing the leachate via pipette. This procedure was repeated 3 times for each sample to maximise the BeF₂ yield.

The high cation loads of pyroxenes complicate Be purification in comparison to quartz samples. Von Blanckenburg et al. (1996) recognised that complexation of trivalent ions with oxalic acid may be used to optimise purification of Be. Oxalic acid forms a large ionic species that does not compete for exchange sites on resin and this approach is now routinely used in quartz samples to effectively remove Ti, Al, and Fe prior to Be elution. To assess our ability to isolate Be in the presence of the heavy cation load presented by pyroxene samples, we calibrated a 20 ml cation exchange column using 100-200 mesh AG50 X8 resin. This resin volume is 4 times greater than our standard procedure for clean quartz samples and acid volumes were scaled accordingly (see Table 3 for final optimised volumes). We measured the concentrations of Be and common contaminants (Ca, Na, Mg, Al, K, Ti, Fe) in the elute from 20 ml acid additions by ICP-MS (Figure 5).

Figure 5 demonstrates how taking up the sample in oxalic acid (cf. von Blanckenburg et al., 1996) effectively removes Al, Ti and Fe, which is important as both Ti and Fe precipitate with Be at pH 9. Be elution peaks after 100 ml of 0.5M HNO₃. The Be peak shown in Figure 4 is relatively clean, although minor overlap with Mg occurs late in the elution. To maximise Be yields we proceeded with a total of 160 ml 0.5 M HNO₃ for all samples herein (Table 3). We revisit the implications of (and possible remedies for) potential Mg contamination in Section 5.

Following cation columns we selectively precipitated BeOH₂ at pH 9 and calcined to BeO, before mixing with Nb powder (BeO 1:4 Nb) and packing into copper targets. ¹⁰Be/⁹Be ratios were measured against the NIST standard with a ¹⁰Be/⁹Be ratio of 3.00 x 10⁻¹¹ on the 14UD tandem accelerator mass spectrometer (AMS) at Australian National University (Fifield et al., 2010). Final ¹⁰Be concentrations are corrected for any procedural contamination by subtracting the number of ¹⁰Be atoms in full chemistry blanks processed alongside the samples and propagating the analytical uncertainties of the blank measurements to those of the sample measurements. The blank measurements contained 25000-77000 ¹⁰Be atoms (Table 4), which range from 0.3 to 50 % (median = 16 %) of the sample totals.

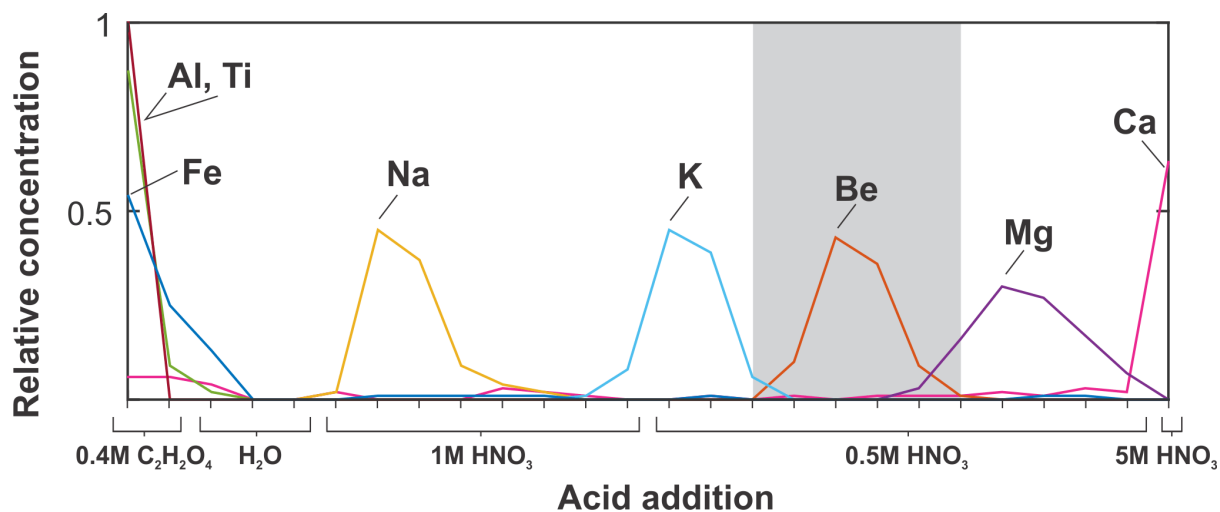


Figure 5: Elution curves for the cation exchange column setup used in this study (20 ml AG50 X8, 100-200 mesh). Measurements took place after each 20 ml eluant addition (x-axis ticks). Grey shading delimits Beryllium elution.

Table 3: Chemical protocol for separating Be from pyroxene

<i>Step</i>	<i>Task description</i>
<i>1</i>	<p><i>Removal of meteoric ^{10}Be</i></p> <ul style="list-style-type: none"> (a) Crush samples to $< 90\ \mu\text{m}$ (b) Weigh sample (c) 10 hr leach in 25 ml in 0.04 M $\text{NH}_2\text{OH}\cdot\text{HCl}$ at 95°C. Leave to cool (d) Centrifuge 5min at 3500 rpm and rinse x3 with leaching solution (e) Transfer to beaker in MilliQ H_2O and dry down (f) Transfer to 50 ml centrifuge tube in 25 ml 1 M HCl and agitate at room temperature $\sim 20^\circ\text{C}$ for 24 hr (g) Centrifuge 5 min at 3500 rpm and rinse using MilliQ H_2O. Repeat x3 (h) Transfer to clean 50 ml centrifuge tube in 35 ml 4 M HF and agitate at 20°C for 24 hr (i) Add 10 ml 15 M HNO_3 and agitate for 20 min at 20°C (j) Dry down sample and weigh. Repeat steps 1h-1i until sample mass reduced by $\sim 20\%$ from 1b.
<i>2</i>	<p><i>Dissolution</i></p> <ul style="list-style-type: none"> (a) Weigh sample precisely (b) Add ^9Be carrier (c) Dissolve overnight in concentrated HF
<i>3</i>	<p><i>BeF_2 leach</i></p> <ul style="list-style-type: none"> (a) Dry down dissolved sample (b) Add 10 ml MilliQ H_2O (c) Heat at 60°C for 20 min then leave to cool (d) Transfer leachate to clean Teflon beaker (e) Repeat steps 3b and 3d three times to maximise BeF_2 yield (f) Dry down sample
<i>4</i>	<p><i>Anion exchange columns - Fe removal</i></p> <ul style="list-style-type: none"> (a) Take up sample in 10 ml 6 M HCl and centrifuge for 5 min at 3500 rpm (b) Prepare 15 ml Eichrom columns with 2 ml Biorad AG1-X8 anion resin (100-200 mesh) <ul style="list-style-type: none"> (i) Add 5 + 5 ml 0.3 M HCl to clean resin (ii) Add 2 + 2 + 2 ml 6 M HCl to condition resin (c) Add sample to column – distribute sample across 2-3 columns if dark in colour (d) Add 2 + 2 + 2 ml 6 M HCl (e) Collect sample and switch to waste collection vessels (f) Add 5 + 5 ml 0.3 M HCl to clean resin – discard to waste (g) Dry down sample
<i>5</i>	<p><i>Cation exchange columns – Be purification</i></p> <ul style="list-style-type: none"> (a) Take up sample in 40 ml 0.4 M oxalic acid and heat at 60°C for ~ 1 hr (b) Allow to cool then centrifuge for 5 min at 3500 rpm (c) Prepare 25 ml Eichrom columns with 20 ml Biorad AG50-X8 cation resin (100-200 mesh) (d) Add 20 + 40 ml 5M HNO_3 to clean resin (e) Add 20 + 20 ml millQ H_2O (f) Add 20 + 40 ml 0.4 M oxalic acid to condition resin (g) Switch collection vessels and add sample (h) Add 20 + 20 ml 0.4 M oxalic acid

-
- (i) Add 200 ml 0.4 M oxalic acid [elute Fe, Al, Ti]
 - (j) Add 20 + 40 ml MilliQ H₂O
 - (k) Add 40 + 60 ml 0.5 M HNO₃ [elute Na] then switch to clean collection vessels
 - (l) Add 20 ml 1 M HNO₃ [elute K], then switch to clean collection vessels
 - (m) Add 80 + 80 ml 1M HNO₃ [elute Be] then switch to waste collection vessels
 - (n) Add 160 ml 5 M HNO₃ to clean resin
 - (o) Add 20 + 20 ml MilliQ H₂O to rinse resin

6 *Be precipitation*

- (a) Dry down Be eluant then transfer to centrifuge tube in 10 ml 1 M HNO₃
- (b) Add conc. ammonia until solution reaches pH 9 (~1 ml)
- (c) Shake vigorously until BeOH flecks form
- (d) Centrifuge 5 min at 3500 rpm to concentrate BeOH gel
- (e) Decante supernate and rinse BeOH in MilliQ H₂O x3

7 *Calcine and prepare AMS targets*

Table 4: Beryllium data for full chemistry blanks processed with the three batches of samples

#	⁹ Be (μg)	Measured ¹⁰ Be/ ⁹ Be ± 1 σ (10 ⁻¹⁵ at. at. ⁻¹)	¹⁰ Be ± 1 σ (10 ³ at.)
1	422.1	0.90 ± 0.50	25.38 ± 14.10
2	372.5	1.39 ± 0.62	34.65 ± 15.53
3	311.5	3.70 ± 1.00	77.00 ± 20.83

3.3 Production rate calibration and exposure age calculations

Cosmogenic nuclide production rates may be constrained in samples using either, independent constraint of the exposure duration (e.g. by radiocarbon, or other geological dating methods), or using coexisting measurements of a second nuclide that has a well-known production rate. Both data types exist for the Murimotu Formation (Eaves et al., 2015) allowing us to constrain the production rate of ¹⁰Be in pyroxene via two independent methods.

We use the radiocarbon age of 10,535 ± 110 cal. yr before AD1950 (BP) for the Murimotu Formation to derive an estimate of the ¹⁰Be production rate in pyroxene using independent age control. We derive these estimates using the online exposure age calculator formerly known as the CRONUS-Earth online production rate calculator, version 3 (Balco, 2017a), available at: http://hess.ess.washington.edu/math/v3/v3_cal_in.html. This calculator computes reference production rates (via spallation) and exposure ages according to three different scaling s (1) ‘St’ – uses the latitude-atmospheric pressure based scaling factors of Stone (2000) and makes no account for temporal variability in the geomagnetic field; (2) ‘Lm’ – uses the latitude-

altitude based scaling factors of Lal (1991) (cf. Balco et al., 2008) modified to account for geomagnetic field variability prescribed according to Lifton (2016); and (3) ‘LSDn’ – an implementation of the nuclide specific scaling scheme described by Lifton et al. (2014). These three schemes produce comparable results at our study sites, thus for simplicity we focus on results from only the ‘Lm’ results in this paper. However, all primary and secondary data inputs and calculated outputs associated with are presented in a supplementary spreadsheet associated with the online version of this manuscript.

Based on field observations our production rate calibrations using the independent age constraints assume zero erosion of the sample surfaces during the extent of their exposure. Cross calibration via a second nuclide, in this case ^3He , allow this assumption to be tested as this technique provides production rate estimates that are independent from biases that can be induced by surface erosion or shielding, as well as temporal variability in the cosmic ray flux at Earth’s surface (Blard et al., 2008). Our cross-calibrated estimated of the *in situ* ^{10}Be production rate in pyroxene is calculated according to the following:

$$P_{10,SLHL} = N_{10} (P_{3,SLHL} / N_3 + \lambda_{10}) \quad (1)$$

Where $P_{10,SLHL}$ and $P_{3,SLHL}$ are the reference production rates of ^{10}Be and ^3He , respectively, at sea level and high latitude ($>60^\circ$), N_{10} and N_3 are the ^{10}Be and ^3He concentrations in the sample, respectively, and λ_{10} is the ^{10}Be decay constant ($4.998 \times 10^{-7} \text{ yr}^{-1}$; Korschinek et al., 2010). For the Murimotu samples, N_3 is taken from Eaves et al. (2015) and both N_3 and N_{10} are corrected for sample thickness and shielding. For $P_{3,SLHL}$ we use the primary calibration set of Borchers et al. (2016), (45 samples from 11 sites, available: <http://calibration.ice-d.org/cds/8>) and use the production rate calibration tools of the online exposure age calculator formerly known as the CRONUS-Earth online exposure age calculator, version 3, to derive $P_{3,SLHL}$ estimates of $127.2 \pm 11.0 \text{ at. g}^{-1} \text{ yr}^{-1}$ (‘Lm’ scaling).

The v.3 production rate calculator produces reference production rates by averaging the samples at individual sites and then, if data are sourced from multiple sites, averaging these site-specific values. For single sites uncertainty represents standard deviation of the individual measurements relative to the averaged value. For multiple sites the standard deviation of all individual samples relative to the site average is compared to the standard deviation of the

individual site averages and the largest of these is assigned. This methodology is designed to avoid weighting results by their measurement uncertainties, which laboratory inter-comparison studies have shown to be underestimated (Jull et al., 2016; Balco, 2017a). For consistency, we follow the v.3 calculator approach to uncertainty assignment when deriving our cross-calibrated reference production rates.

As reference production rate estimates are rare for ^{10}Be in pyroxene, we also combine our results with two previous estimates derived from lava flows on Mt. Etna (Blard et al., 2008). These two samples also have both independent age control, derived from K/Ar dating, as well as coexisting measurements of cosmogenic ^3He (Blard et al., 2005). We recalculate production rates for these samples in the same manner described above and data is compiled in the Supplementary Data File.

For exposure ages of the Mt. Gran samples we also use the online exposure age calculator formerly known as the CRONUS-Earth online exposure age calculator, version 3, available at: <http://hess.ess.washington.edu/>. We note that the muon scheme implemented in this calculator is developed for quartz (Balco, 2017b), thus we are assuming that production of ^{10}Be in pyroxene by muons is similar to that in quartz. Given the minor contribution of muonic production in surface samples we consider this assumption reasonable pending phase-specific constraints.

4. Results

4.1 Production rate constraints for ^{10}Be in pyroxene

In situ cosmogenic ^{10}Be concentrations in pyroxenes from the Murimotu debris avalanche range from $0.57 \pm 0.1 \times 10^5$ to $1.36 \pm 0.2 \times 10^5$ at. g $^{-1}$ (Table 1). After correcting for differences in sample thickness and topographic shielding (Table 5) these four samples fail a chi-squared goodness-of-fit test ($\chi^2=16.7$, 3d.f., $p<.05$) at the 95 % confidence interval, which indicates low probability that the inter-sample variability can be explained by analytical uncertainty alone. Sample MM-12-03 yielded a ^{10}Be concentration that was more than 2 standard deviations greater than the population mean, indicating that it may be an outlier. Eaves et al. (2015) also

highlighted sample as a potential outlier based on its deviation from the mean of cosmogenic ^3He concentrations. However, in the case of ^3He , this sample yielded a concentration that was lower than the population mean, which led Eaves et al. (2015) to suggest that the parent boulder may have lost nuclides due to post-depositional surface erosion. Due to these uncertainties, and because different surface samples were processed for ^3He and ^{10}Be (Figure 2a), we omit this sample from further consideration here. Variability in the remaining three samples can be explained by measurement uncertainty alone ($\chi^2 = 3.3$, 2 d.f. $p > .05$).

Using the independent ^{14}C age for the Murimotu debris avalanche (10535 ± 110 cal. yr BP, $n=8$; Eaves et al., 2015) and the arithmetic mean ^{10}Be concentration ($7.41 \pm 1.84 \times 10^4$ at. g^{-1} ; $n=3$), we derive a local production rate in pyroxene of 7.0 ± 1.8 at. $\text{g}^{-1} \text{yr}^{-1}$ at the Murimotu site. Converting this to a reference (sea-level, high latitude) ^{10}Be production rate using the Lm scaling scheme yields 3.5 ± 0.9 at. $\text{g}^{-1} \text{yr}^{-1}$. Combining the ^{10}Be concentrations with the existing ^3He measurements yields $^3\text{He}/^{10}\text{Be}$ ratios of 45 ± 9 , 25 ± 5 , and 38 ± 8 and cross-calibrated estimates of $P_{10,SLHL}$ (see equation 1) of 2.9 ± 0.6 to 5.1 ± 1.1 at. $\text{g}^{-1} \text{yr}^{-1}$, with an average for the Murimotu site of 3.7 ± 1.2 at. $\text{g}^{-1} \text{yr}^{-1}$ (Lm scaling; Table 5).

Two previous measurements of ^{10}Be in pure pyroxene separates exist from two separate lava flows from Mt Etna (Blard et al., 2008). These lavas are supported by independent age constraints derived using K/Ar dating (Blard et al., 2005), which yield reference production rates of 2.7 ± 0.6 and 3.5 ± 0.9 at. $\text{g}^{-1} \text{yr}^{-1}$ (Table 5) and are consistent with our estimates from the New Zealand site. Combining these extra constraints with our data yields a combined reference production rate for ^{10}Be of 3.2 ± 0.8 at. $\text{g}^{-1} \text{yr}^{-1}$ (Lm scaling; Table 5). Cross calibrated estimates of $P_{10,SLHL}$ are similarly consistent with the Murimotu samples (Table 5) and yield a combined, cross-calibrated reference production rate estimate of 3.6 ± 0.8 at. $\text{g}^{-1} \text{yr}^{-1}$ (Lm

scaling; $n=5$). All production rate estimates for Murimotu ($n=3$) or Murimotu plus Mt Etna ($n=5$) samples are pass a χ^2 goodness-of-fit test at the 95 % confidence level.

4.2 Exposure dating application at Mt Gran, Mackay Glacier, Antarctica

We compute surface exposure ages using $P_{10,SLHL}$ for pyroxene derived using independent age data and scaled using the time-dependent ‘Lm’ scaling scheme (3.2 ± 0.8 at. g.⁻¹ yr¹). Application of the compiled production rate presented above to ¹⁰Be measurements in pyroxenes from glacial cobbles at Mt. Gran yields exposure ages ranging from 32.0 ± 8.3 ka to 5.5 ± 4.0 ka (1σ internal uncertainties; Table 6). The high uncertainties in these exposure ages reflect the relatively low analytical precision of the ¹⁰Be/⁹Be measurements (Table 1), which range from 17 to 34 % (median = 23 %), and in some cases the magnitude of the blank correction.

Samples MG12 (15.9 ± 3.2 ka) and MG30 (12.8 ± 4.9 ka) are from the same elevation (1043 m above mean sea level; 116 m above the present glacier surface) at the top of our vertical transect and yield ages that are indistinguishable from one another within the 1σ analytical uncertainties). Sample MG01 represents the lowermost sample of our transect (970 m above mean sea level; 29 m above the present glacier surface) and yields an exposure age of 5.4 ± 4.0 ka – the youngest of the transect. Together these samples bracket the ~100 m vertical elevation transect between 14.3 ± 2.2 ka (arithmetic mean \pm standard error of the mean of samples MG12 and MG030) and 5.5 ± 4.0 ka (MG01). In general the dataset exhibits a general decreasing trend in exposure duration from the transect top towards the ice surface (Figure 6). All samples except MG07 return ages that are stratigraphically coherent (i.e. the exposure age is younger than the overlying sample and older than the next lowest sample within the 1σ uncertainty

403 level) with ice surface lowering between uppermost and lowermost bracketing ages (Figure 6;
404 Table 6).

Table 5: Compilation of co-existing measurements of ^{10}Be and ^3He in mafic minerals, with cross-calibrated (via ^3He) productions rates for ^{10}Be . Cosmogenic isotope concentrations have been corrected for sample thickness and shielding as reported in source publications (see Supplementary Data File). $P_{3,\text{SLHL}}$ used for cross calibration is taken as the globally compiled cosmogenic ^3He production rate of $127.8 \pm 11.6 \text{ at. g}^{-1} \text{ yr}^{-1}$ (St scaling) and $127.2 \pm 11.0 \text{ at. g}^{-1} \text{ yr}^{-1}$ (Lm scaling). All uncertainties are 1σ .

Source / name	Phase	^{10}Be (10^4 at. g^{-1})	^3He (10^6 at. g^{-1})	$^3\text{He}/^{10}\text{Be}$	$P_{10,\text{SLHL}} - \text{ind. age,}$ Lm scaling (at. $\text{g}^{-1} \text{ yr}^{-1}$)	$P_{10,\text{SLHL}} - \text{cross-}$ cal.via ^3He , Lm scaling (at. $\text{g}^{-1} \text{ yr}^{-1}$)	Cross-calibration/ Independent age	Source(s)
<u>Murimotu Formation debris avalanche, New Zealand ($10.6 \pm 0.1 \text{ ka}$)</u>								This study; Eaves et al. (2015)
MM1201	px	5.79 ± 1.2	2.61 ± 0.1	45 ± 9	2.7 ± 0.5	2.8 ± 0.6	1.0 ± 0.3	
MM1202	px	9.40 ± 1.7	2.36 ± 0.1	25 ± 5	4.5 ± 0.8	5.1 ± 1.0	1.1 ± 0.3	
MM1203	px	13.8 ± 1.8	2.11 ± 0.1	15 ± 2	6.7 ± 0.9	8.3 ± 1.3	1.2 ± 0.3	
MM1204	px	7.00 ± 1.4	2.68 ± 0.1	38 ± 8	3.4 ± 0.7	3.3 ± 0.7	1.0 ± 0.3	
Murimotu (n=3)	px			36 ± 10	3.5 ± 0.9	3.7 ± 1.2	1.1 ± 0.1	
<u>Nave lava flow, Mt Etna, Italy</u>								
SI41 ($33 \pm 2 \text{ ka}$)	px	15.5 ± 3.3	5.94 ± 0.3	38 ± 8	2.7 ± 0.6	3.4 ± 0.8	1.3 ± 0.4	Blard et al. (2005, 2008)
SI27a ($32 \pm 4 \text{ ka}$)	70 % px 30 % ol	27.6 ± 2.1	7.38 ± 0.4	27 ± 3		4.9 ± 0.6		
<u>Piano Della Lepre flow, Mt Etna Italy ($10 \pm 3 \text{ ka}$)</u>								Blard et al. (2005, 2008)
SI43	px	14.3 ± 3.2	5.07 ± 0.4	35 ± 8	3.5 ± 0.9	3.7 ± 0.9	1.0 ± 0.4	
<u>Mauna Kea moraine, Hawaii</u>								Blard et al. (2007, 2008)
MK11	ol	46.7 ± 7.5	1.24 ± 0.5	27 ± 4		4.8 ± 0.9		
<u>Haleakala lava flow, Hawaii</u>								Nishiizumi et al. (1990)
M-85-5	ol	109 ± 33	3.6 ± 1.1	36 ± 11		3.6 ± 1.1		
Px_only (n=5)				37 ± 7	3.2 ± 0.8	3.6 ± 0.8	1.1 ± 0.1	
Ol_only (n=2)				28 ± 11		4.2 ± 1.1	4.2 ± 1.1	
Px_ol_all (n=8)				33 ± 11		4.0 ± 1.2	4.0 ± 1.2	

406

Table 6: Exposure ages from glacial cobbles at Mt Gran derived using the compiled reference ('Lm' scaling) production rate for ^{10}Be in pyroxene of 3.2 ± 0.8 at $\text{g}^{-1} \text{yr}^{-1}$. Sample identified as outliers are denoted by italics.

Sample	Age $\pm 1\sigma$ int. uncertainty (ka)	Elevation above modern ice surface (m)
MG30	15.9 ± 3.2	116
MG32	12.8 ± 4.9	114
<i>MG07</i>	32.0 ± 8.3	86
MG12	12.3 ± 3.5	82
<i>MG15</i>	18.0 ± 4.8	62
MG19	9.8 ± 5.4	47
MG22	9.4 ± 3.7	50
MG01	5.5 ± 4.0	29

407

408 5. Discussion

409 We have replicated the decontamination procedure of Blard et al. (2008), demonstrating that
 410 meteoric ^{10}Be is removed successfully from our samples after ~ 2 hydrofluoric acid leaches,
 411 which reduced the sample mass by $\sim 20\%$ (Figure 4). Previous, unsuccessful attempts to isolate
 412 *in situ* ^{10}Be in pyroxene crystals used dolerite samples from the Sirius Group sediments in
 413 Antarctica (Ivy-Ochs et al., 1998), which have independently-derived exposure durations of ~ 2
 414 Myr. Ivy-Ochs et al. (1998) attribute the difficulty in removing meteoric ^{10}Be from these
 415 samples to the long exposure times, which increases the content of weathering products such
 416 as clays in the crystal interior, which may host meteoric ^{10}Be . Both our study and that of Blard
 417 et al. (2008) achieved successful removal of meteoric ^{10}Be from pyroxene samples that have
 418 comparatively short exposure durations (< 35 kyr), which is consistent with the weathering-
 419 based contamination hypothesis.

420

Nishiizumi et al. (1990) successfully isolated *in situ* ^{10}Be in olivine crystals from a ~500 ka lava flow using only the standard decontamination procedures developed for quartz. Despite shorter exposure durations, the weathering rate at this tropical site should be greater than the Antarctic samples of Ivy-Ochs et al. (1998). The different levels of success in meteoric ^{10}Be removal between these two studies may be due to differences in the crystal structures of pyroxene and olivine that may enhance and reduce, respectively, the potential for meteoric ^{10}Be to penetrate the crystal lattices. For example, the well-defined cleavage planes of pyroxene, which are not present in olivine crystals, may offer pathways for the penetration of meteoric ^{10}Be . We suggest that future attempts to isolate *in situ* ^{10}Be from pyroxene with long exposure times, or high weathering rates, should first verify meteoric ^{10}Be removal in a test sample using the sequential dissolution method (e.g. Figure 4a; Seidl et al., 1997; Blard et al., 2008).

Our application of the Be decontamination method to pyroxenes from the Murimotu debris avalanche at Mt. Ruapehu volcano in New Zealand yielded a reference production rate of $3.5 \pm 0.9 \text{ at. g}^{-1} \text{ yr}^{-1}$ ($n=3$, ‘Lm’ scaling; Table 5) using the independent radiocarbon-based constraint for this deposit (Eaves et al., 2015). This estimate for $P_{10,\text{SLHL}}$ in pyroxene is in good agreement with two previous production rate estimates from Mt Etna (Blard et al., 2008), which, when combined with our data, give a compiled ($n=5$) reference production rate of $3.2 \pm 0.8 \text{ at. g}^{-1} \text{ yr}^{-1}$ (‘Lm’ scaling). Calibrated production rates from all pyroxene samples are indistinguishable, within 1σ uncertainties, from those derived via cross-calibration with ^3He (Table 5), which supports our inference of negligible surface erosion of our samples.

Application of this new pyroxene-based ^{10}Be production rate estimate to dolerite cobbles deposited on Mt Gran by the Mackay Glacier yields a relatively coherent vertical transect recording ~100 m ice surface lowering. Only sample MG07 yields an exposure age that exceeds

those of its surrounding samples by greater than the 1σ analytical uncertainties (Figure 6; Table 6). It is probable that this sample inherited some ^{10}Be from a previous period of exposure, which can be common in Antarctica where cold-based ice fails to sufficiently erode rock surfaces (e.g. Hein et al., 2014). We thus consider MG07 unreliable for constraint of the duration of most recent exposure, which, according to the remaining samples, appears to have occurred between ~14 and 6 ka.

A previous exposure dating campaign, using ^{10}Be in quartz from cobbles from nunataks protruding the lower portions of this glacier, identified a phase of rapid thinning that occurred at ~7 ka when the glacier surface lowered from ~230 to 25 m above present (Figure 6a). The mean and standard error (1σ) of the quartz samples that are situated in the same sample elevation bracket (relative to the present ice surface) as the Mt Gran pyroxene samples is 7.0 ± 0.8 ka ($n=15$; Figure 6b; Supplementary Data File). Of the 7 pyroxene samples (after MG07 is removed), 5 have external uncertainty ranges (1σ) that overlap with this quartz-defined time window of rapid thinning. It also noteworthy that flowline model simulations of the Mackay Glacier (Jones et al., 2015) predict that ice surface lowering at Mt Gran, in response to grounding line retreat, may precede that at the nunataks downstream from which the quartz samples were taken. This effect may explain the separation of the pyroxene and quartz chronologies in the upper reaches of our transect (Figure 6b). The pyroxene based chronology at Mt Gran is thus broadly consistent with that derived from quartz in cobbles from nearby nunataks. However, we refrain from making any definitive evaluation of the reference ^{10}Be production rate for pyroxene based on this comparison, as the overlap between the pyroxene and quartz samples could largely result from the low analytical precision of the pyroxene measurements.

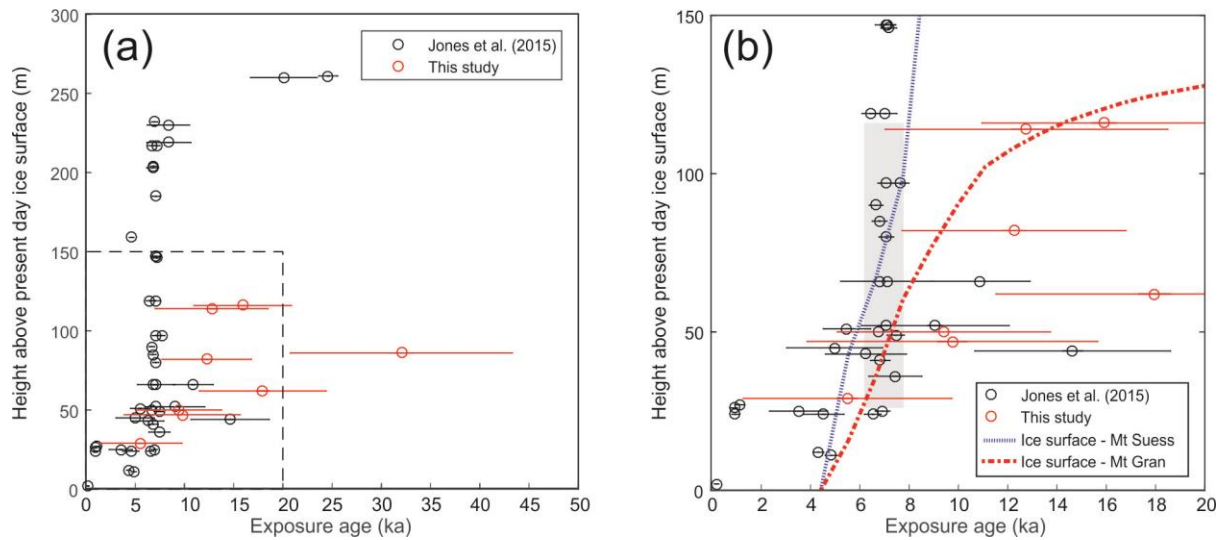


Figure 6: Pyroxene-derived exposure ages at Mt Gran (red; $n=8$; this study) and quartz-based exposure ages of Jones et al. (2015) (black; $n=44$). Ages are plotted with 1 s.d. external uncertainty). Dashed rectangle in panel (a) delineates the axes limits of panel b. Grey bar in panel b denotes the arithmetic mean and standard error of the mean (7.0 ± 0.8 ka; $n=15$) of quartz-based ages situated within the same elevation range (116-26 m, above the present ice surface) of the pyroxene-based samples. Also shown are the ice surface elevation profiles at Mt Suess (blue dashed line) and Mt Gran (red dashed line) taken from the transient flowline model simulations of Jones et al. (2015).

The analytical precision achieved in this study (11-34 %; Table 1) is comparable with previous measurements of *in situ* ^{10}Be in pyroxene and olivine (Nishiizumi et al., 1990; Seidl et al., 1997; Blard et al., 2008). However this level of precision is considerably lower than other, more commonly-used cosmogenic nuclide-mineral pairs (e.g. $\ll 10$ % for *in situ* ^{10}Be in quartz). After blank correction, the uncertainties on the final ^{10}Be concentrations range from 20 to 72 %, which are high even before uncertainties in the production rate are included. Our process blanks are not unusually high ($\sim 30\text{-}80 \times 10^3$ atoms) which suggests that, in the near term, applications of this mineral-nuclide pair may be better suited to samples with greater ^{10}Be content that are less sensitive to blank corrections (i.e. longer exposure durations or higher local production rates).

It is clear that the analytical precision must be improved further for ^{10}Be in pyroxene to become a viable alternative or complementary nuclide-mineral pair for geological applications. One avenue for improving AMS counting statistics and reducing the analytical uncertainties of ^{10}Be concentrations is to increasing the pyroxene mass digested for Be extraction provides. In this study, we dissolved up to 2.8 g of pyroxene per sample (Table 1), which represented a compromise between maximising the total number of ^{10}Be atoms available for measurement, while minimising the cationic content of contaminant elements (e.g. Mg, Ti). Increasing the sample mass much beyond this level would mean greater expense of time and materials for pyroxene separation and cation-exchange column processing. Relatively weak correlation between sample mass and analytical precision ($r^2=0.34$) of our *in situ* ^{10}Be measurements suggests that efforts to reduce analytical uncertainties may be more effectively focused on improving the quality and consistency of Be purification, which, in turn, will facilitate processing of greater sample masses

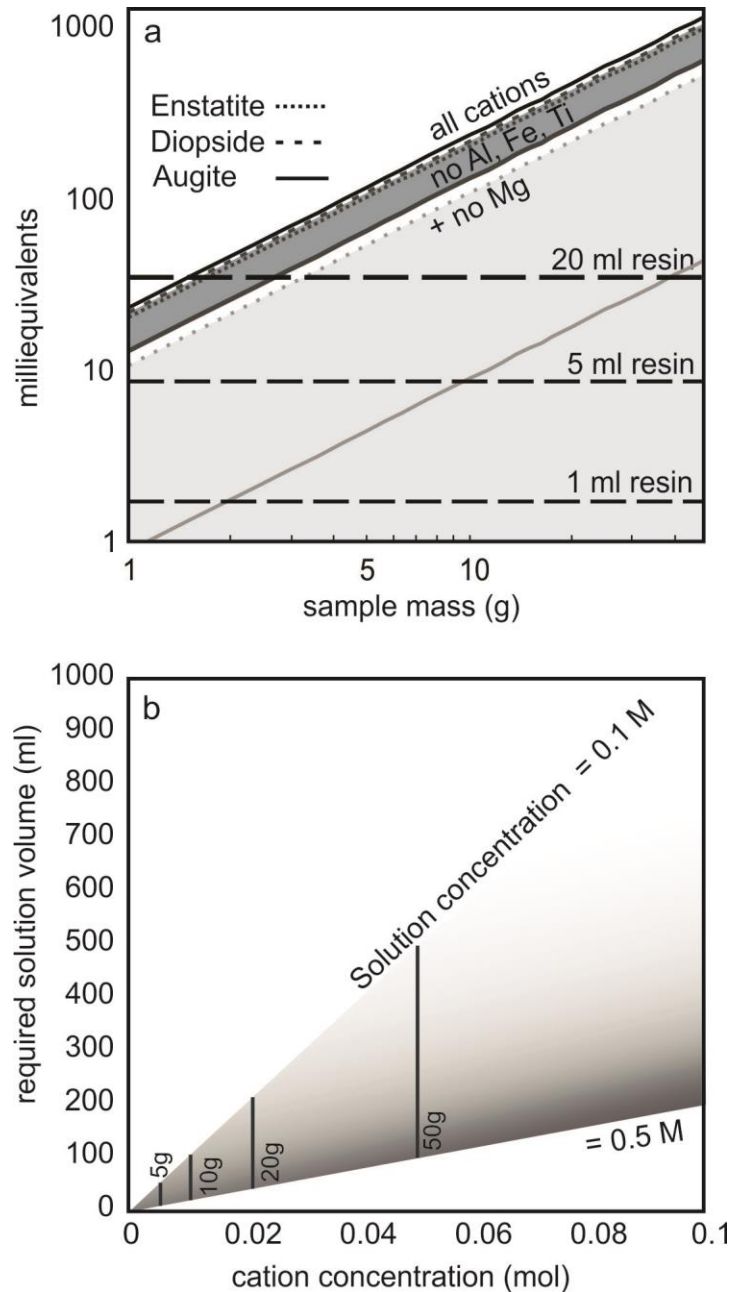


Figure 7: Exchange resin and precipitation optimisations for pyroxene. a) Cation milliequivalents are shown for all cations (black), no Al, Fe, Ti (i.e. the case where trivalent cations are complexed with oxalic acid (von Blanckenburg et al, 1996, dark grey), and the hypothetical case whereby Mg is to be removed by high-pH precipitation prior to cation columns (light grey)). Endmember pyroxene compositions for Enstatite (dotted lines, MgSiO_3), Diopside (dashed lines, CaSiO_3), and Augite (solid lines, $\text{CaMgSi}_2\text{O}_6$) are shown. b) Exchange resin volumes required for varying cationic loads held in 0.1-0.5 M solution. Estimated cationic loads of selected pyroxene masses are also indicated.

Our cation column calibration experiment demonstrated how standard oxalic acid procedures developed for quartz (von Blankenburg et al., 1996) effectively removed Fe, Ti, and Al, allowing separation of up to 2.8 g of pyroxene in 20 ml of cation resin (Figure 7). Further improvement in Be purification may be achieved by addressing the overlap of Be and Mg that occurs late in the Be elution (Figure 7). This overlap is particularly significant for ^{10}Be -pyroxene applications as Mg is present in non-negligible concentrations of many pyroxene types. Seidl et al. (1997) stated that acetylacetone extraction, undertaken after cation exchange columns, was required to sufficiently isolate Be from Mg in olivine samples. In that study, the authors processed between 5 and 11 g of olivine, and achieved consistent analytical precision of ~12 %, although the *in situ* ^{10}Be concentrations were between 2 and 10 times higher than in our study. Using the same chemical procedure Shepard et al. (1995) report exposure ages from ^{10}Be measurements in 2.5-8 g olivine olivine that have ~20 % uncertainties.

Perhaps a simpler alternative approach to extraction via organic solvents could be to precipitate Mg as brucite at high pH before cation exchange columns. This modification would have the dual benefits of reducing the contaminant load and allowing processing of larger sample masses while maintaining workable volumes of resin and without compromising Be yields (Figure 7a). Ochs and Ivy Ochs (1997) calculated speciation in mixed solutions for a variety of common cations. They showed that Be and Al precipitate at ~pH 9 while Mg remains in solution. Similarly, at high pH, Be and Al become soluble while Mg precipitates. For the 50W-X8 resin used in our study, ~1.7 meq. ml^{-1} resin, ~20 ml of resin would be required to contain all the cations of Augite if Al, Fe, and Ti are complexed with oxalic acid. For the pyroxene series, 20 g of pyroxene would yield ~0.02 mol of cations. The speciation calculations performed by Ochs and Ivy Ochs (1997) are only valid for total cation concentrations of 0.1 to 0.5 M. As such, large volumes of solution might be required for precipitations (Figure 7b). In order to

ensure complete precipitation of Mg at high pH, between 40 and 200 ml of solution is needed for the 20 g sample (Figure 7b). The volumes are more manageable for 5 g of pyroxene, requiring at most 50 ml of solution, which suggests that 5 g may be reliably processed through these methods.

6. Conclusions

Previous attempts to extract and measure *in situ* ^{10}Be from pyroxene have yielded mixed results. We have successfully replicated the procedure for meteoric ^{10}Be decontamination outlined by Blard et al (2008) and optimised cation exchange column separation of the *in situ* ^{10}Be component. Our results suggest that measurement of *in situ* ^{10}Be from pyroxene can be routine, – at least for young (c. 10^2 – 10^5 yr) mafic terrains - thus providing a potential alternative or complementary nuclide-mineral pair for geological applications. Applications where samples have been exposed for long durations (e.g. $>10^4$ yr) should first seek to verify successful decontamination of accumulated weathering products that may host meteoric ^{10}Be using the experimental design of Blard et al. (2008).

Using a well-dated volcanic debris avalanche deposit in New Zealand we have further constrained the reference production rate for ^{10}Be in pyroxene, yielding results (3.5 ± 0.9 at. $\text{g}^{-1} \text{yr}^{-1}$ ($n=3$; ‘Lm’ scaling) that are indistinguishable from previous estimates. Combining these data yields a globally-compiled reference production rate for ^{10}Be in pyroxene of 3.2 ± 0.8 at. $\text{g}^{-1} \text{yr}^{-1}$ ($n=5$; ‘Lm’ scaling). Applying this production rate to ^{10}Be concentrations in pyroxene from Ferrar Dolerite erratics at Mackay Glacier, Antarctica, we produced a stratigraphically coherent chronology of ice surface lowering. The pyroxene based chronology indicates ~100 m of ice surface lowering at this site occurred between ~14 and 6 ka which is in agreement with a quartz based ^{10}Be chronology that shows strong evidence for rapid thinning at ~7 ka, as

well as glacier flowline model experiments. However, the pyroxene-based chronology is hampered by high analytical uncertainties, which would limit any glaciological interpretations if this method was applied at this site in isolation.

It is clear from our results that the future viability of ^{10}Be in pyroxene for geological applications requires (i) improved analytical precision, and (ii) further constraint of the production rate to reduce the uncertainties below the present level ($\sim 20\%$). The former may be achievable in applications to samples with Be concentrations (e.g. $> 10^6$ at. g^{-1}), such as those exposed for longer durations or situated at higher elevations. However, our experiments also highlight that methodological improvements, such as reducing Mg contamination in Be cathodes, may yield noticeable improvements in measurement precision. Improved constraint of reference production rates requires addition of further geological and cross-calibration data to refine our understanding of *in situ* ^{10}Be production in pyroxene. Existing cosmogenic ^3He calibration sites (e.g. as compiled in Goehring et al., 2018) represent obvious first targets.

Acknowledgements

This research was funded by a Victoria University Research Fund grant awarded to KPN and ANM.

References

- Balco, G. 2017a. Documentation -- v3 exposure age calculator. Available: <https://sites.google.com/a/bgc.org/v3docs/home> [Accessed August 2018]
- Balco, G. 2017b. Production rate calculations for cosmic-ray-muon-produced ^{10}Be and ^{26}Al benchmarked against geological calibration data. *Quaternary Geochronology*, 39, 150-173.

Balco, G., Stone, J.O., Lifton, N.A. and Dunai, T.J., 2008. A complete and easily accessible means of calculating surface exposure ages or erosion rates from ^{10}Be and ^{26}Al measurements. *Quaternary Geochronology*, 3(3), pp.174-195.

Blard, P.H., Lavé, J., Pik, R., Quidelleur, X., Bourles, D. and Kieffer, G., 2005. Fossil cosmogenic ^3He record from K–Ar dated basaltic flows of Mount Etna volcano (Sicily, 38°N): evaluation of a new paleoaltimeter. *Earth and Planetary Science Letters*, 236(3), pp.613-631.

Blard, P.H., Lavé, J., Pik, R., Wagnon, P. and Bourlès, D., 2007. Persistence of full glacial conditions in the central Pacific until 15,000 years ago. *Nature*, 449(7162), p.591.

Blard, P.H., Bourles, D., Pik, R. and Lavé, J., 2008. *In situ* cosmogenic ^{10}Be in olivines and pyroxenes. *Quaternary Geochronology*, 3(3), pp.196-205.

Borchers, B., Marrero, S., Balco, G., Caffee, M., Goehring, B., Lifton, N., Nishiizumi, K., Phillips, F., Schaefer, J. and Stone, J., 2016. Geological calibration of spallation production rates in the CRONUS-Earth project. *Quaternary Geochronology*, 31, pp.188-198.

Conway, C.E., Leonard, G.S., Townsend, D.B., Calvert, A.T., Wilson, C.J., Gamble, J.A. and Eaves, S.R., 2016. A high-resolution $^{40}\text{Ar}/^{39}\text{Ar}$ lava chronology and edifice construction history for Ruapehu volcano, New Zealand. *Journal of Volcanology and Geothermal Research*, 327, pp.152-179.

Eaves, S.R., Winckler, G., Schaefer, J.M., Vandergoes, M.J., Alloway, B.V., Mackintosh, A.N., Townsend, D.B., Ryan, M.T. and Li, X., 2015. A test of the cosmogenic ^3He production rate in the south-west Pacific (39° S). *Journal of Quaternary Science*, 30(1), pp.79-87.

Eaves, S.R., Mackintosh, A.N., Anderson, B.M., Doughty, A.M., Townsend, D.B., Conway, C.E., Winckler, G., Schaefer, J.M., Leonard, G.S. and Calvert, A.T., 2016a. The Last Glacial Maximum in the central North Island, New Zealand: palaeoclimate inferences from glacier modelling. *Climate of the Past*, 12, pp.943-960.

Eaves, S.R., Mackintosh, A.N., Winckler, G., Schaefer, J.M., Alloway, B.V. and Townsend, D.B., 2016b. A cosmogenic ^3He chronology of late Quaternary glacier fluctuations in North Island, New Zealand (39 S). *Quaternary Science Reviews*, 132, pp.40-56.

Fenton, C.R., Niedermann, S., Goethals, M.M., Schneider, B. and Wijbrans, J., 2009. Evaluation of cosmogenic ^3He and ^{21}Ne production rates in olivine and pyroxene from two Pleistocene basalt flows, western Grand Canyon, AZ, USA. *Quaternary Geochronology*, 4(6), pp.475-492.

Fifield, L.K., Tims, S.G., Fujioka, R., Hoo, W.T. Everett, S.E. 2010. Accelerator mass spectrometry with the 14UD accelerator at the Australian National University. *Nuclear Instruments and Methods in Physics Research*, B268, pp.858-862.

Goehring, B.M., Kurz, M.D., Balco, G., Schaefer, J.M., Licciardi, J. and Lifton, N., 2010. A reevaluation of *in situ* cosmogenic ^3He production rates. *Quaternary Geochronology*, 5(4), pp.410-418.

Goehring, B.M., Muzikar, P. and Lifton, N.A., 2018. Establishing a Bayesian approach to determining cosmogenic nuclide reference production rates using He-3. *Earth and Planetary Science Letters*, 481, pp.91-100.

Gosse, J.C. and Phillips, F.M., 2001. Terrestrial *in situ* cosmogenic nuclides: theory and application. *Quaternary Science Reviews*, 20(14), pp.1475-1560.

Hein, A.S., Fogwill, C.J., Sugden, D.E., Xu, S., 2014. Geological scatter of cosmogenic-nuclide exposure ages in the Shackleton Range, Antarctica: Implications for glacial history. *Quaternary Geochronology* 19, 52-66.

Ivy-Ochs, S., Kubik, P.W., Mazarik, J., Wieler, R., Lauper, B. and Schlüchter, C., 1998. Preliminary results on the use of pyroxene for ^{10}Be surface dating. *Schweizerische mineralogische und petrographische Mitteilungen*, 78, pp.375-382.

Jones, R., Mackintosh, A., Norton, K.P., Golledge, N.R., Fogwill, C., Kubík, P.W., Christl, M., Greenwood, S.L., 2015. Rapid Holocene thinning of an East Antarctic outlet glacier driven by marine ice sheet instability. *Nature communications* 6, 8910.

Jull, A.T., Scott, E.M. and Bierman, P., 2015. The CRONUS-Earth inter-comparison for cosmogenic isotope analysis. *Quaternary Geochronology*, 26, pp.3-10.

Korschinek, G., Bergmaier, A., Faestermann, T., Gerstmann, U.C., Knie, K., Rugel, G., Wallner, A., Dillmann, I., Dollinger, G., Von Gostomski, C.L. and Kossert, K., 2010. A new value for the half-life of ^{10}Be by heavy-ion elastic recoil detection and liquid scintillation counting. *Nuclear Instruments and Methods in Physics Research Section B: Beam Interactions with Materials and Atoms*, 268(2), pp.187-191.

Lal, D., 1991. Cosmic ray labeling of erosion surfaces: *in situ* nuclide production rates and erosion models. *Earth and Planetary Science Letters*, 104(2-4), pp.424-439.

Lifton, N., 2016. Implications of two Holocene time-dependent geomagnetic models for cosmogenic nuclide production rate scaling. *Earth and Planetary Science Letters*, 433, pp.257-268.

Lifton, N., Sato, T. and Dunai, T.J., 2014. Scaling *in situ* cosmogenic nuclide production rates using analytical approximations to atmospheric cosmic-ray fluxes. *Earth and Planetary Science Letters*, 386, pp.149-160.

Mirsky, A., Treves, S.B., Calkin, P.E., 1965. Stratigraphy and Petrography, Mount Gran Area, Southern Victoria Land, Antarctica, *Geology and Paleontology of the Antarctic. American Geophysical Union*, pp. 145-175.

Niedermann, S. 2002. Cosmic-ray-produced noble gases in terrestrial rocks: dating tools for surface processes. In: D. Porcelli, C.J. Ballentine, R. Wieler (Eds.), *Noble Gases in Geochemistry and Cosmochemistry*, Rev. Min. Geochem, vol. 47, pp. 731–784

Nishiizumi, K., Klein, J., Middleton, R., Craig, H., 1990. Cosmogenic ^{10}Be , ^{26}Al , and ^3He in olivine from Maui lavas. *Earth and Planetary Science Letters* 98, 263–266.

- Ochs, M. and Ivy-Ochs, S., 1997. The chemical behavior of Be, Al, Fe, Ca and Mg during AMS target preparation from terrestrial silicates modeled with chemical speciation calculations. *Nuclear Instruments and Methods in Physics Research Section B: Beam Interactions with Materials and Atoms*, 123(1-4), pp.235-240.
- Palmer, B.A. and Neall, V.E., 1989. The Murimotu Formation—9500 year old deposits of a debris avalanche and associated lahars, Mount Ruapehu, North Island, New Zealand. *New Zealand Journal of Geology and Geophysics*, 32(4), pp.477-486.
- Putnam, A.E., Schaefer, J.M., Barrell, D.J.A., Vandergoes, M., Denton, G.H., Kaplan, M.R., Finkel, R.C., Schwartz, R., Goehring, B.M. and Kelley, S.E., 2010. *In situ* cosmogenic ¹⁰Be production-rate calibration from the Southern Alps, New Zealand. *Quaternary Geochronology*, 5(4), pp.392-409.
- Schäfer, J.M., Ivy-Ochs, S., Wieler, R., Leya, I., Baur, H., Denton, G.H. and Schlüchter, C., 1999. Cosmogenic noble gas studies in the oldest landscape on earth: surface exposure ages of the Dry Valleys, Antarctica. *Earth and Planetary Science Letters*, 167(3), pp.215-226.
- Schimmelpfennig, I., Benedetti, L., Garreta, V., Pik, R., Blard, P.H., Burnard, P., Bourles, D., Finkel, R., Ammon, K. and Dunai, T., 2011. Calibration of cosmogenic ³⁶Cl production rates from Ca and K spallation in lava flows from Mt. Etna (38°N, Italy) and Payún Matru (36°S, Argentina). *Geochimica et Cosmochimica Acta*, 75(10), pp.2611-2632.
- Shepard, M.K., Arvidson, R.E., Caffee, M., Finkel, R. and Harris, L., 1995. Cosmogenic exposure ages of basalt flows: Lunar Crater volcanic field, Nevada. *Geology*, 23(1), pp.21-24.
- Seidl, M.A., Finkel, R.C., Caffee, M.W., Hudson, G.B. and Dietrich, W.E., 1997. Cosmogenic Isotope Analyses Applied to River Longitudinal Profile Evolution: Problems and Interpretations. *Earth Surface Processes and Landforms*, 22(3), pp.195-209.
- Stone, J. (1998). A Rapid Fusion Method for Separation of Beryllium-10 From Soils and Silicates. *Geochimica et Cosmochimica Acta*, 62, 551-561.

Stone, J.O., 2000. Air pressure and cosmogenic isotope production. *Journal of Geophysical Research: Solid Earth*, 105(B10), pp.23753-23759.

Sugden, D., Denton, G., 2004. Cenozoic landscape evolution of the Convoy Range to Mackay Glacier area, Transantarctic Mountains: onshore to offshore synthesis. *Geological Society of America Bulletin* 116, 840-857.

Tost, M. and Cronin, S.J., 2016. Climate influence on volcano edifice stability and fluvial landscape evolution surrounding Mount Ruapehu, New Zealand. *Geomorphology*, 262, pp.77-90.

Townsend, D.B., Leonard, G. S., Conway, C.E., Eaves, S.R., Wilson, C. J. N., compilers 2017. Geology of the Tongariro National Park Area [map]. Lower Hutt (NZ): GNS Science. 1 sheet + 109 p., scale 1:60 000. (GNS Science geological map; 4).

von Blanckenburg, F., Belshaw, N.S. and O'Nions, R.K., 1996. Separation of ⁹Be and cosmogenic ¹⁰Be from environmental materials and SIMS isotope dilution analysis. *Chemical Geology*, 129(1-2), pp.93-99.

von Blanckenburg, F. and Willenbring, J.K., 2014. Cosmogenic nuclides: Dates and rates of Earth-surface change. *Elements*, 10(5), pp.341-346.

Zerathe, S., Blard, P.H., Braucher, R., Bourlès, D., Audin, L., Carcaillet, J., Delgado, F., Benavente, C., Aumaître, G. and Keddadouche, K., 2017. Toward the feldspar alternative for cosmogenic ¹⁰Be applications. *Quaternary Geochronology*, 41, pp.83-96.